Numerical modeling of the churning power losses in planetary gearboxes: An innovative partitioning-based meshing methodology for the application of a computational effort reduction strategy to complex gearbox configurations

Franco Concli[1] | Carlo Gorla[2]

Thanks to the recent developments in the computer science, simulations are becoming an increasingly widespread approach that can help the designers in the development of new products. In the specific field of gearboxes, simulations are used mainly for structural evaluations. However, while for the structural design beside the simulations, many analytical methods and international standard are available; for the prediction of the power losses and the efficiency of gears, neither accurate analytical methods nor automated simulation tools are available. The authors work on this topic since years and have developed new methodolo-gies based on computational fluid dynamics. With respect to general purpose commercial software, these techniques allow a significant reduction of the com-putational effort and have the capability to take into account particular physical phenomena that occurs in gears, such as cavitation, and for which no information are available in literature. The purpose of this paper is to introduce a new auto-mated mesh-partitioning strategy implemented to extend the applicability of the previously developed computational effort reduction method to complex gear-boxes getting over the geometrical limitations adopted in the past. To show the capabilities of this new strategy, we simulated a planetary gearbox that represents at the same time one of the most complicated kinematic arrangements of gears and the configuration for which the numerical fluid dynamics simulation can give the major contribution both with planar simplified models as well as with com-plete 3D models.

KEYWORDS: CFD, churning, gear, meshing, planetary, squeezing

1 | INTRODUCTION

In the recent decades, the international trends suggest to reduce the power dissipation and to increase the efficiency. Solutions that are more efficient introduce important benefits not only for cost savings but also for impact on the environment. In the specific field of mechanical transmissions, higher efficiency is strongly related to an improved reliability of the system. For all these aspects, the gearbox manufacturers are continuously pushing in this sense.

Received: 28 November 2016
Revised: 2 February 2017
Accepted: 5 February 2017

[1] Faculty of Science and Technology, Free University of Bozen-Bolzano, Italy
[2] Mechanical Engineering Dept., Politecnico di Milano, Milan, Italy

Correspondence
Franco Concli, Faculty of Science and Technology, Free University of Bolzano, piazza Università, 5 I-39100 Bolzano, Italy. Email: franco.concli@unibz.it

The optimization of the gearbox efficiency is traditionally performed using, during the design stage, analytical-empirical models for the different sources of loss. Once the first prototypes were manufactured and assembled, a significant experimental effort for the final optimization of the internal shapes of the gearbox as well as for the optimization of the lubricant level is necessary.

The power dissipation of a gearbox is a consequence of different sources of loss related to the various mechanical components such as gears, bearings, seals, etc. The losses related to the gear sliding as well as the bearing losses have been deeply studied in the past and reliable models allow a precise estimation of the dissipations. On the other side, the load independent losses generated by the gears (due to the interaction with the lubricant) cannot be accurately quantified. This aspect limits also the accuracy of the global efficiency predictions due to the uncertainty on the churning losses and reduces the capability of optimization. The various models that can be found in literature, in fact, are experimentally derived and, consequently, can be applied only to a confined range of operating conditions. Furthermore, often some important parameters were not taken into account by those models. The first works performed by Daily et al,[1] Mann et al,[2] and Soo et al,[3] for example, can only be applied to a single gears, disks or bladed rotors. Additional models were proposed by Terekhov,[4] Lauster et al,[5] and more recently, Boness[6] and Changenet et al.[7] Terekhov developed empirical relations for different dip lubricated gear geometries. Walter[8] subsequently extended the original equations proposed by Terekhov. Starting from these results, Mauz[9] studied the load independent losses of gearboxes. Even if the equations proposed by Mauz are still considered the most complete available model, they does not take into account important parameters such as the helix angle that can have a huge impact on the power losses as demonstrated by the author.[10]

Recently, different authors among which Marchesse et al,[11] Hill et al,[12] and Gorla et al[13] applied computational fluid dynamic (CFD) for such purposes. The results of different researches have shown the effectiveness of the CFD approach for the characterization and the optimization of the power losses of gears.[14–20] The CFD allows to model each specific operating conditions and design overcoming the main limitation of the empirical models. On the other side, the computational effort needed for such calculation has represented a substantial limitation to the wide diffusion of this approach. Recently the authors have presented an innovative mesh handling technique[21,22] that leads to a substantial reduction of the simulation time. In the considered example (Forschungsstelle für Zahnräder und Getriebebau (FZG) test rig), the computational time was reduced by 93.5% with respect to the state-of-the-art. However, this new mesh-handling technique is applicable only to simple geometries such as, for example, single stages parallel axis gearboxes. In this paper, an evolution of such technique is presented and applied to a practical example. The goal is to extend the applicability of the method to each gearbox configuration. For this purposes, a specific partitioning strategy was implemented. Thanks to arbitrary mesh interfaces (AMIs), it was possible to simulate in a reasonable amount of time a complete planetary gearbox that represent one of the most complex gearbox configurations and in which the load independent power losses of gears play the biggest role.

1.1 | Power losses

The power dissipation inside a gearbox is the sum of the power losses generated by different mechanical components. It can be, therefore, distinguish between losses related to gears, bearings, seals, and other components such as, for example, clutches and synchronizers. The gear and bearing losses can be furtherly subdivided into load dependent and load independent. The load dependent losses are directly proportional to the transmitted load and are associated to the sliding between the different mechanical components. The so-called load-independent power losses[23] are not directly proportional to the transmitted load but indirectly affected by a variation of the lubricant properties with the temperature induced by the load dependent losses. These losses arise because of the interaction of the lubricant and the mechanical components. But while for bearings which geometry is standardized, the manufacturers provide trustable equations to estimate the power dissipation, for the gears which arrangement depends from the specific configuration of the gearbox, only numerical methods seems to be able to provide reliable and accurate results.

1.2 | Numerical approach

So as to predict the lubricant behavior and, consequently, the load independent power losses, the internal fluid dynamic should be solved. The numerical solution of the fluid domain inside the gearbox is performed with a finite volume method. This relies on the solution of 2 governing equations that mathematically represent the mass and momentum conservation

$$\frac{\partial \rho}{\partial t} + \nabla\cdot(\rho \boldsymbol{v}) = 0, \tag{1}$$

$$\frac{\partial (\rho \boldsymbol{v})}{\partial t} + \nabla\cdot(\rho \boldsymbol{v}\boldsymbol{v}) = -\nabla p + \nabla\cdot\left[\mu\left(\nabla \boldsymbol{v} + \nabla \boldsymbol{v}^T\right)\right] + \rho \boldsymbol{g} + \boldsymbol{F}, \tag{2}$$

in which ρ is the density, $\boldsymbol{v}$ is the velocity vector, μ the viscosity, $\boldsymbol{g}$ is the gravity vector, and $\boldsymbol{F}$ represents the external forces. These basic equations describe the behavior of a

transient incompressible flow and should be applied to each cell in which the computational domain is discretized.

The solution of the system of equation is performed with numerical techniques based on a PIMPLE (merged PISO-SIMPLE) algorithm.[22]

The SIMPLE algorithm (developed for steady-state conditions) is effective but does not contain temporal information. On the contrary, the PISO algorithm (developed for transient simulations) is time conservative but, to ensure convergence of the solution, the time step should be reduced causing a significant increase in the computational effort. The PIMPLE algorithm operates like the SIMPLE one for all the iterations except the last one in which operates in PISO mode. In this manner, it is possible to conjugate a good stability of the solution without loss of information with a reduced computational effort.

So as to take into account the presence of more than one phase (dip lubrication), an additional scalar quantity called volume fraction α is introduced. For each cell, this quantity is calculated with an additional balance equation.

$$\frac{\partial}{\partial t}\alpha + \frac{\partial}{\partial x_i}(\alpha u_i) = 0. \tag{3}$$

Once the volume fraction is computed, in each cell, the so called "mixture properties" are computed as an averaged mean of the properties of the different phases.

$$\phi = \phi_g \cdot \alpha + \phi_l \cdot (1-\alpha), \tag{4}$$

where ϕ represents the generic property such as, for instance, the density or the viscosity and the subscripts g and l stand for gas and liquid, respectively.

A relatively recent development uses a compressive scheme for the discretization of the gaseous volume fraction α. An artificial supplementary velocity field $\boldsymbol{v}_C$ is defined in the proximity of the interface in such a way that the local flow steepens the gradient of the volume fraction function and the interface resolution is improved. A number of different approaches to define the compressive velocity field are reported in literature, eg, compressive interface capturing scheme for arbitrary meshes as described by Ubbink[24] and the currently used multidimensional universal limiter with explicit solution,[25] which limits the flux of the variables to guarantee a bounded solution.

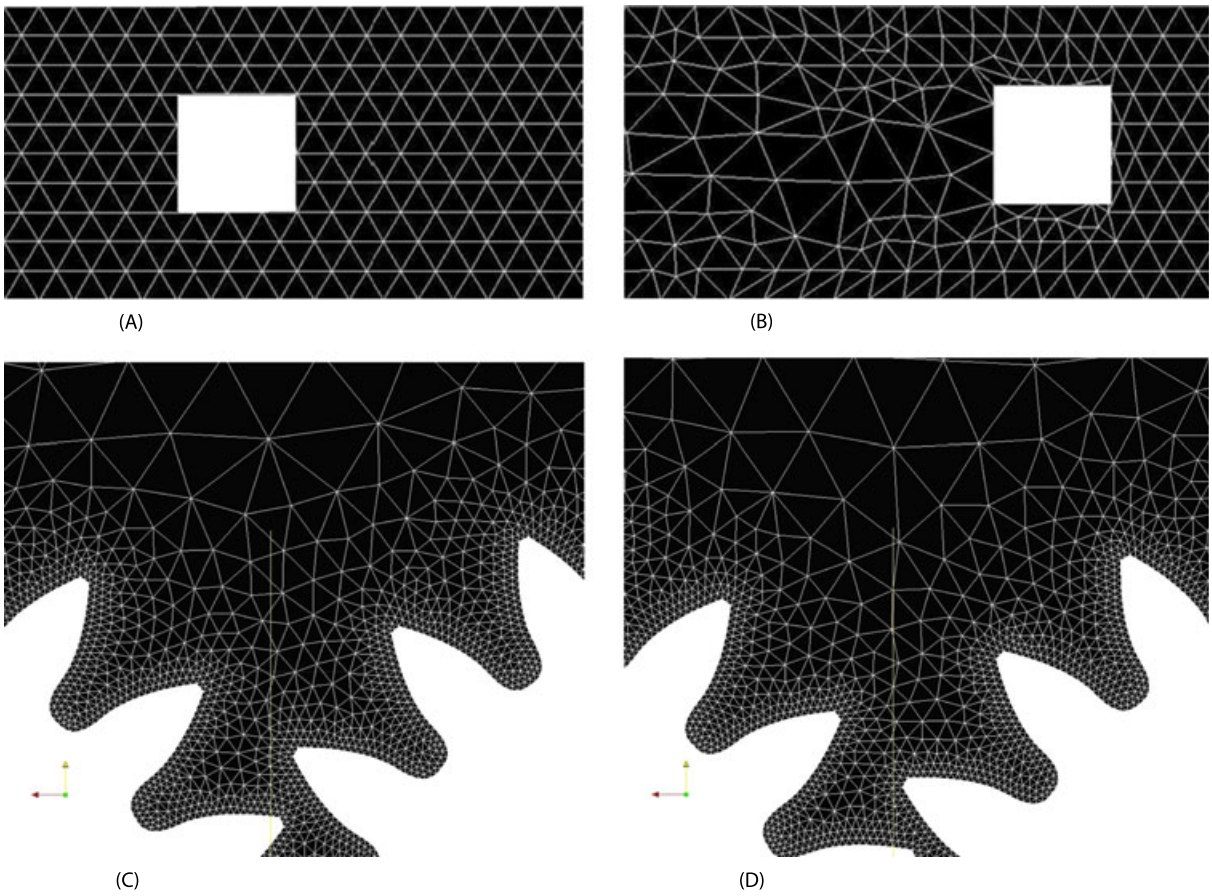

FIGURE 1 Mesh before and after the update: A and B, Local remeshing. C and D, Global remeshing [Colour figure can be viewed at wileyonlinelibrary.com]

1.3 | Mesh-handling techniques

The main difficulty in the simulation of the internal lubrication of gearboxes is related to the intrinsic topological modification of the domain during operations, which requires to update the computational grid after few time steps to counteract the mesh quality degeneration and prevent the numerical instability of the solution. The most widely diffused technique implemented in commercial software called "local remeshing"[26] is based on a first mesh smoothing (idealization of the mesh as a network of interconnected springs) and a subsequent local replacement of the elements which quality does not satisfy the selected criteria. This method is effective and is able to manage big topological modifications but is not efficient. Often the newly generated element results significantly smaller than the initial ones imposing a sudden reduction of the time steps (to ensure the solution stability) with a significant impact on the computational effort.

Recently the author has proposed a new mesh-handling technique that relies on the complete mesh substitution (so-called global remeshing) after few iterations and the mapping of the results between the grids. The generation of the new grids can be better controlled than the regeneration of the distorted elements ensuring a more homogeneous element size and quality.

Figure 1 shows how the local remeshing, also for simple topological modifications produces very small and/or distorted elements while the new approach[21] is capable to maintain the mesh quality also for complex geometrical modifications such as mating gears.

Both methods, local and global remeshing, are based on 2-dimensional tetrahedral meshes successively extruded. This is the limiting factor that prevents the direct application of such method to "complex" gearbox configurations. This method was successfully applied in the past for the simulation of an FZG test rig.[23]

The domain made by half (thanks to symmetry) of the test gearbox was partitioned axially into 2 subdomains. The midplane was meshed following a top down strategy that starts by computing the corner points, and discretize the edges and the faces with an advancing front surface mesh generator. A fast Delaunay algorithm generates the mesh. Eventually it fails for the last elements, back-tracking rule-based algorithm takes over.[27,28] This initial planar mesh with 3 internal partitions (corresponding to the lateral surfaces of the gears and the remaining area that surrounds the gears) was extruded in the 2 directions so to create the final grid (the partitions corresponding to the gear flanks are extruded just in 1 direction while the remaining partition in both directions). This technique is very powerful; the mesh generation takes just few seconds even for a 0.5M cells mesh; but when more complex geometries are considered, this method cannot be directly applied if not with a 2D approximation.

For this reason, considering the importance to simulate the lubrication and the power dissipation of real applications, the author integrates a new and innovative partitioning-based meshing technique to the already presented global remeshing method so to be able to apply such extrusion strategy to each possible gearbox design. In particular, a planetary gearbox was selected as test case (Figure 2). This was first simulated with the 2-dimensional approximation and then in 3 dimensions.

The considered gearbox is a single stage planetary reducer in which the ring gear is fixed. Three planets transmit the power from the sun gear (input shaft) to the planet carrier, which is made by a solid shaft (output) and a counter plate (Figure 2). The planets are mounted with full complement bearings on pins fitted by interference in the planet carrier and the counter plate. The main geometrical

TABLE 1 Main geometrical parameters

m_n [mm]	0.8	z_1[−]	12	m_n [mm]	0.7	z_1[−]	27
α_n [°]	20	z_2[−]	47	α_n [°]	20	z_2[−]	40
i [−]	10	z_3[−]	−108	i [−]	5	z_3[−]	−108

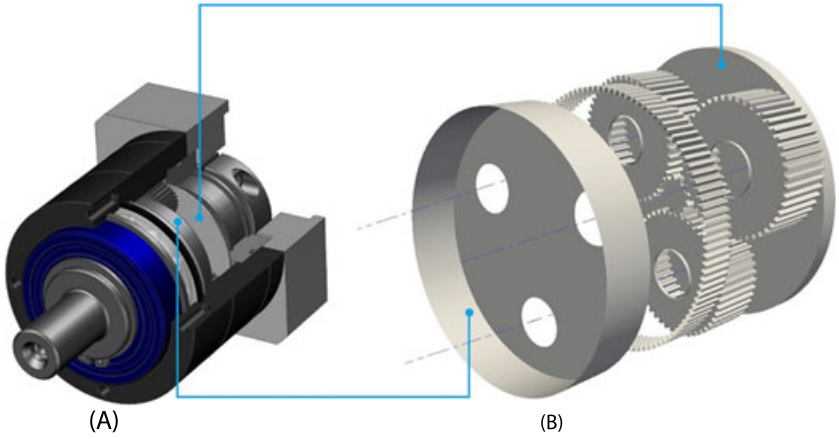

FIGURE 2 A, Layout of the considered planetary gearbox. B, Numerical model [Colour figure can be viewed at wileyonlinelibrary.com]

parameters of the gearbox (in 2 configurations) are listed in Table 1.

Two-dimensional simulations were performed considering the symmetry plane of the gears. Such kind of simulations, even very low time consuming, is useful only for a rough estimation of the power dissipation because they neglect secondary source of losses such as those on the lateral sides of the gears and the planet carrier.

To be able to apply the previously described "global remeshing" strategy to the 3-dimensional case, we subdivided the computational domain into 7 axial partitions according to Figure 3. The black lines represent the interfaces

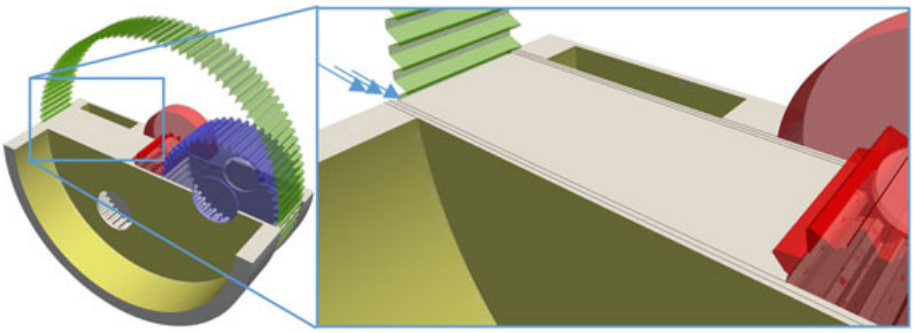

FIGURE 3 Details of the partition strategy [Colour figure can be viewed at wileyonlinelibrary.com]

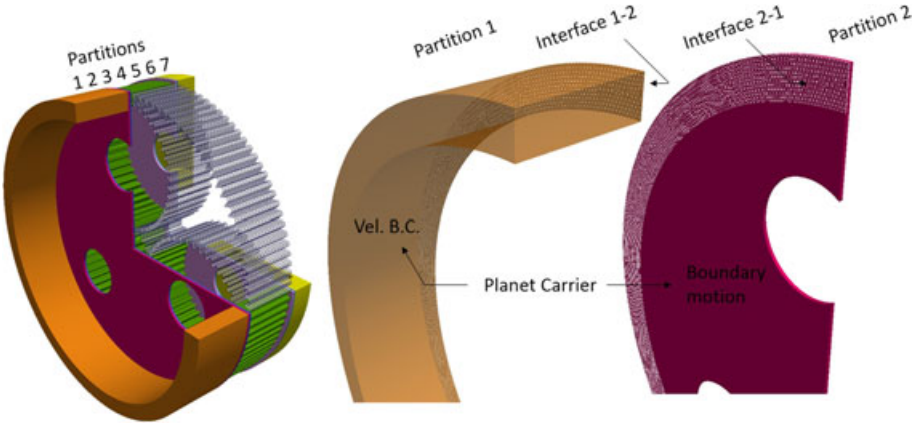

FIGURE 4 Schematization of the partitioning and the arbitrary mesh interface structure [Colour figure can be viewed at wileyonlinelibrary.com]

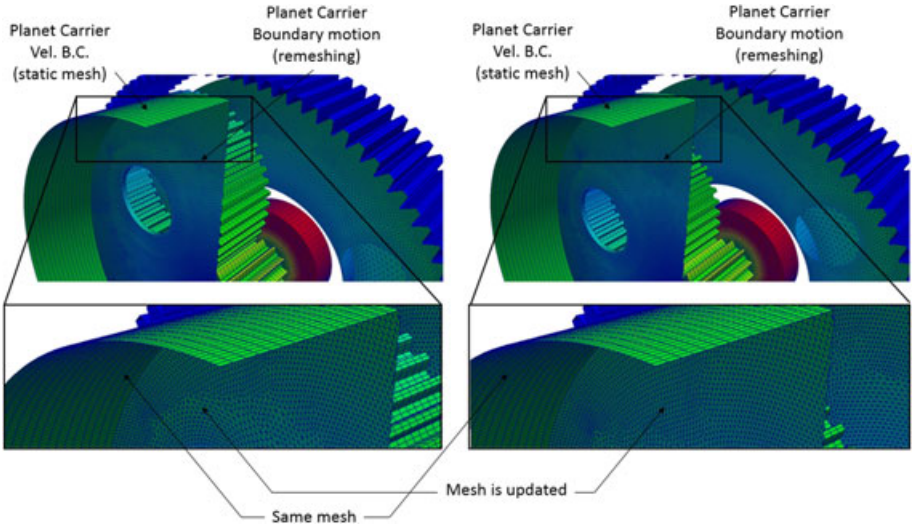

FIGURE 5 Boundary motion and boundary conditions [Colour figure can be viewed at wileyonlinelibrary.com]

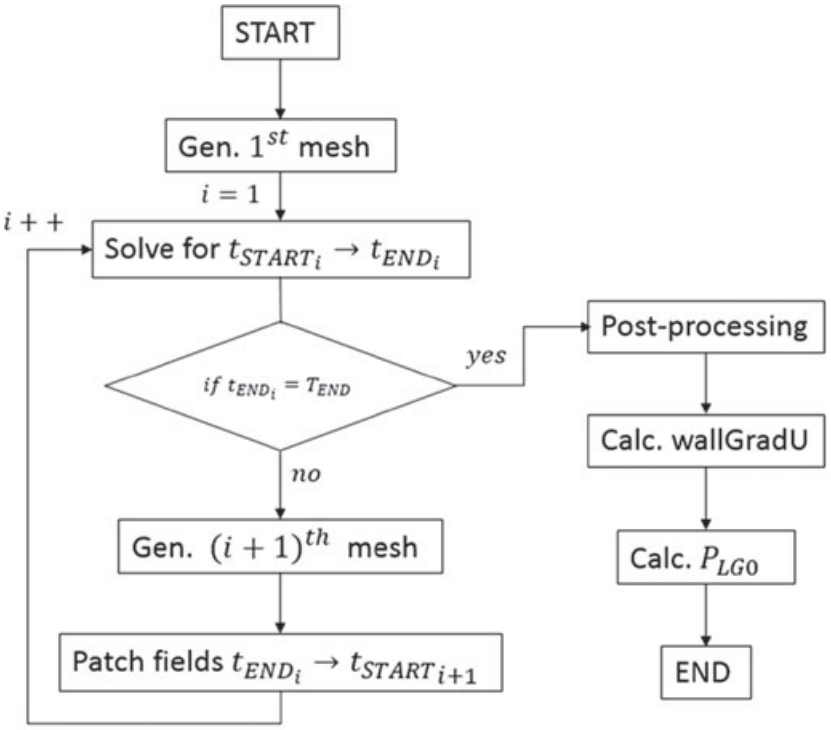

(A)

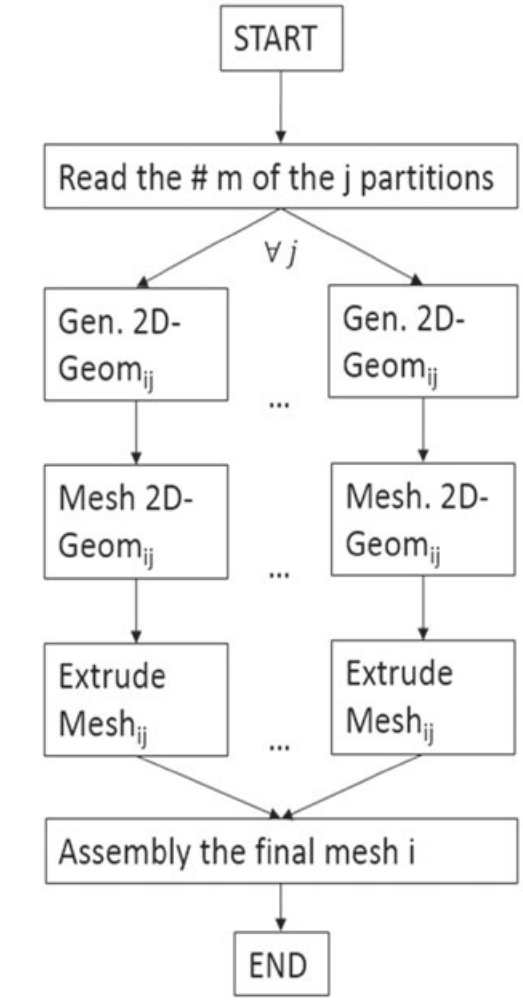

(B)

FIGURE 6 A, Automatic simulation procedure flowchart. B, Meshing procedure flowchart

between the different partitions. Each partition is discretized with an extruded mesh. The procedure relies on an automatized algorithm that, for a prescribed time step, generates the planar geometries for each partition. These are then discretized and the resulting grid extruded. Each sector (partition) of the global grid is generated and meshed separately and can be handled by a different CPU so to speed up the meshing procedure.

As consequence of this, while the geometries at the interfaces are conformal, the meshes are not. Through the introduction of an AMI, the different partitions (disconnected from a geometrical point of view) result numerically connected. This ensures that during the simulations the field variables remain the same at both sides of the interfaces.

The AMI for non-conformal patches has been implemented based on the algorithm described in Farrell and Maddison.[29] The AMI is a technique that allows simulation across disconnected, but adjacent, mesh domains. The domains can be stationary or move relative to one another.

Figure 4 shows the AMI between the first 2 partitions.

1.4 | Automatic procedure

The simulation tool was implemented in the OpenFOAM environment.[30] While the fluid dynamic solver was already available, the algorithm for the boundary motion, the automatization of the mesh generation and update, as well as the assembly of the different partitions was newly developed. As accurately described in Concli and Gorla,[22] before each time step, all the dictionaries that control the simulation were automatically modified. The fluid dynamic is solved upon a prescribed time for which the mesh reaches the maximum acceptable distortion.

During each time steps, only the motion of the boundaries is known and prescribed. The points that belong to the sun gear as well as the lateral sides of the planet carrier and its counter plate are rotated (boundary motion). The planets and the supporting pins, instead, are subjected to a rototranslation that derives from their mounting position eccentric with respect to the planet carrier axis. A dedicated algorithm able to apply a rototranslation to the boundaries was coded and included in the model. The boundaries corresponding to the radial surfaces of the planet carrier and its counter plate in the lateral partitions does not move. Their rotation is modeled with the application of a tangential speed (velocity boundary condition). This shrewdness allows to use the initial meshes of the 2 lateral partition (#1 and 7) for the whole simulation without the need of remeshing them (Figure 5).ensuring a time saving.

The internal vertexes of the grid, those not falling on moving boundaries, must adapt their position in order to follow the boundary motion and to preserve the mesh validity

TABLE 2 Calculated power losses—2D simulations

Lubricant[a] Level	P_{LG0} [W]	
	$i = 10$	$i = 5$
Low 25%	1	1.5
Med. 50%	2	5
High 75%	3.5	15

[a]Klübersynth GH-6 220 θ = 50

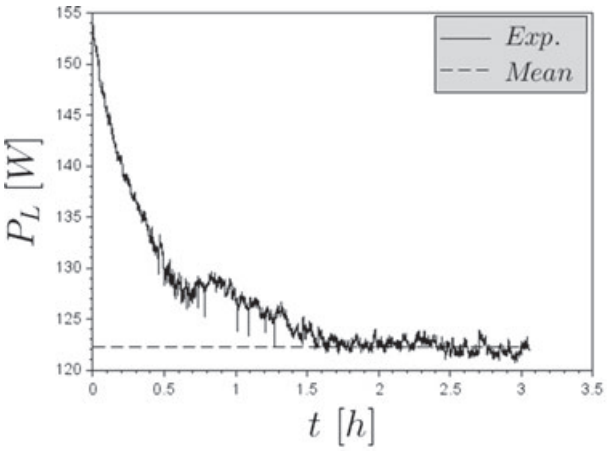

(A) experimental results according to [30]

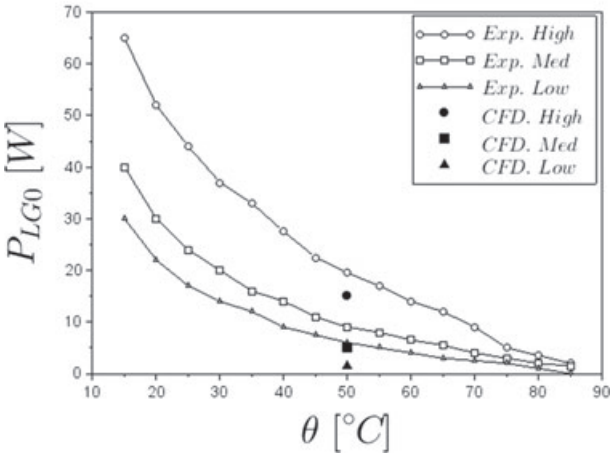

(B) experimental results according to [18]

FIGURE 7 Experimental results according to A, OpenFOAM[30] and B, Concli and Gorla[18]

TABLE 3 The churning due to the rototranslation vs the total churning given by the planets

Lubricant Level	$P_{LG0,satT}/P_{LG0,sat}$ [−]	
	$i = 10$	$i = 5$
Low	9%	21%
Medium	16%	27%
High	20%	33%

upon the next mesh substitution. A typical algorithm for the internal point motion is based on the solution of the point diffusivity equation. Points are therefore moved solving a diffusion point motion equation as follows:

$$\gamma \nabla^2 \boldsymbol{x} = 0, \tag{5}$$

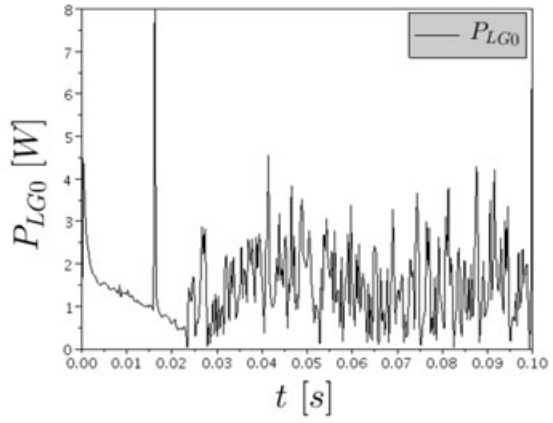

(A)

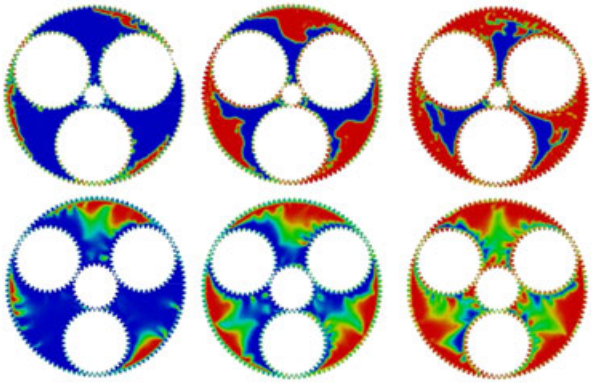

(B)

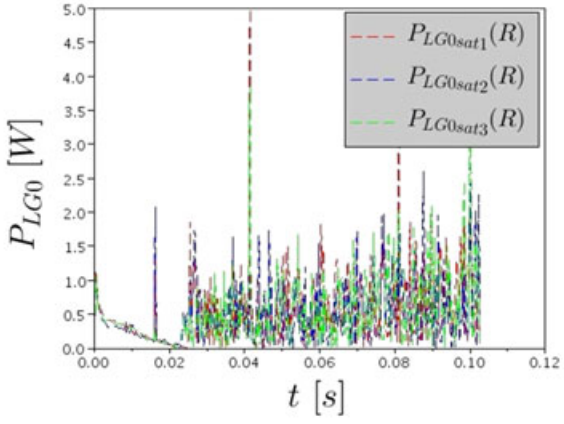

(C)

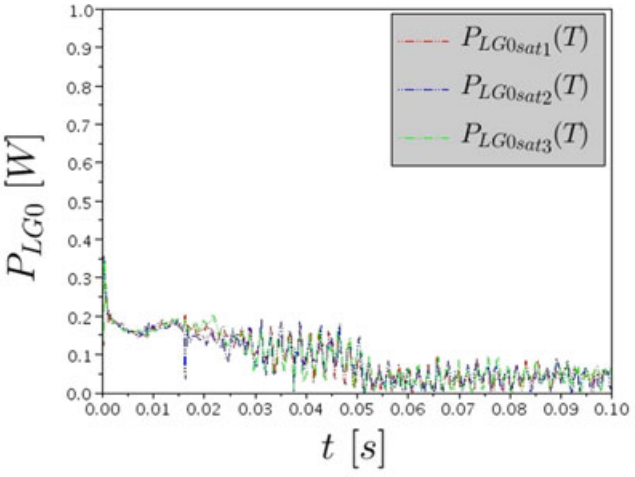

(D)

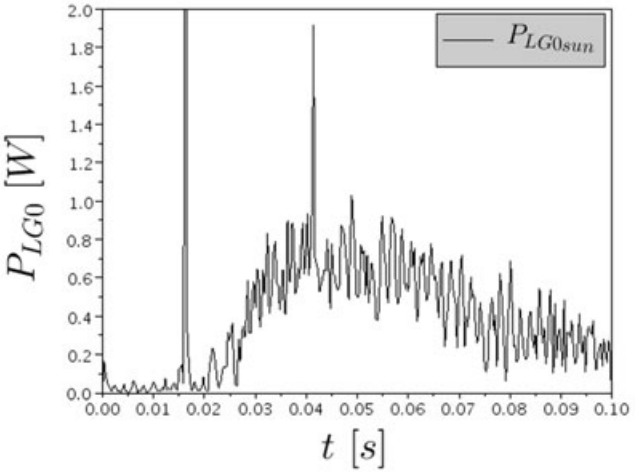

(E)

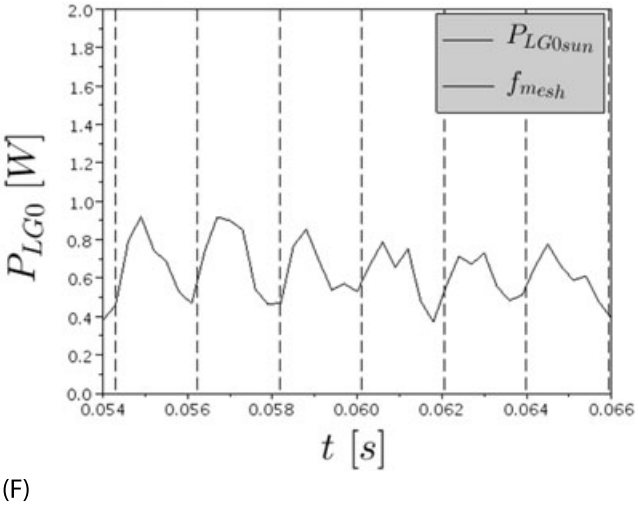

(F)

FIGURE 8 Two-dimensional simulation: ratio 10. Lubricant level: low. A, Total hydraulic losses. B, Lubricant distribution. C, Planets power losses due to rotation. D, Planets power losses due to translation. E, Sun gear losses. F, Sun gear losses (detail) [Colour figure can be viewed at wileyonlinelibrary.com]

where the coefficient γ is the diffusion coefficient that is evaluated according to the inverse of the distance from the points to specified boundary patches. This means that points close to specific patches are moved similarly to boundary nodes, points far from the boundary patches are moved with a small displacement.

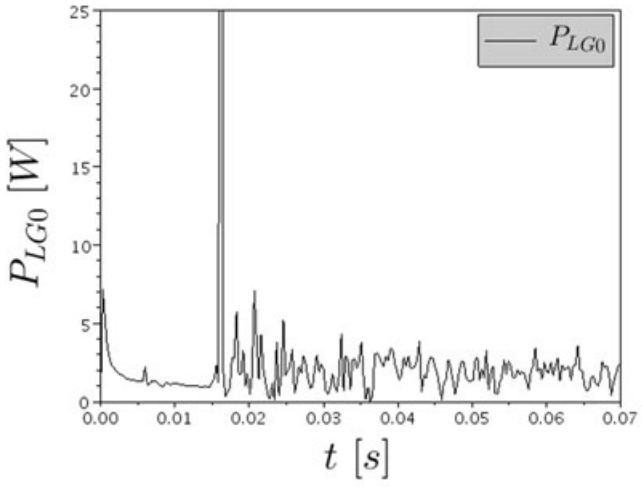

(A)

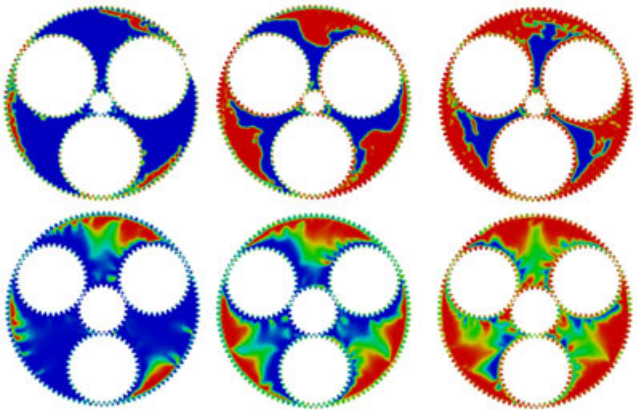

(B)

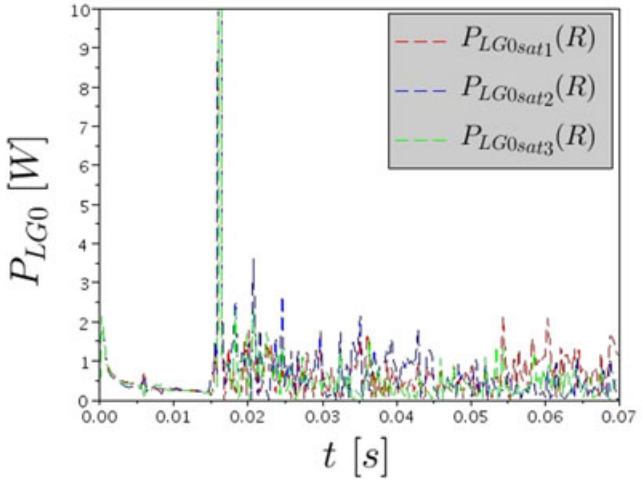

(C)

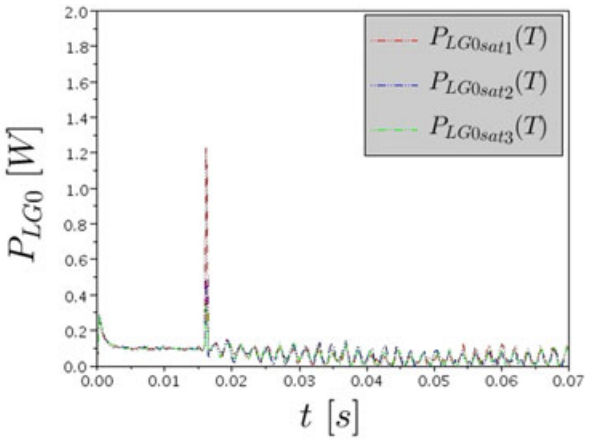

(D)

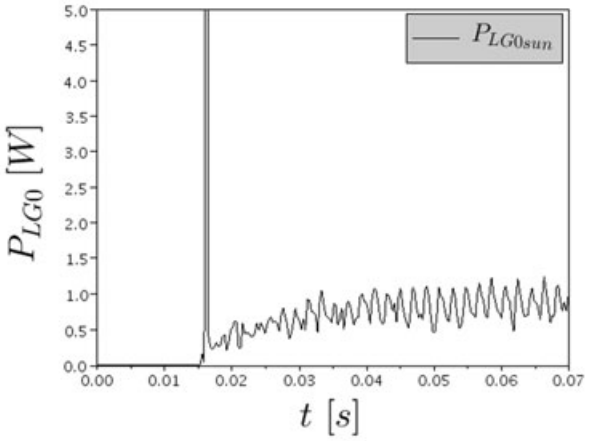

(E)

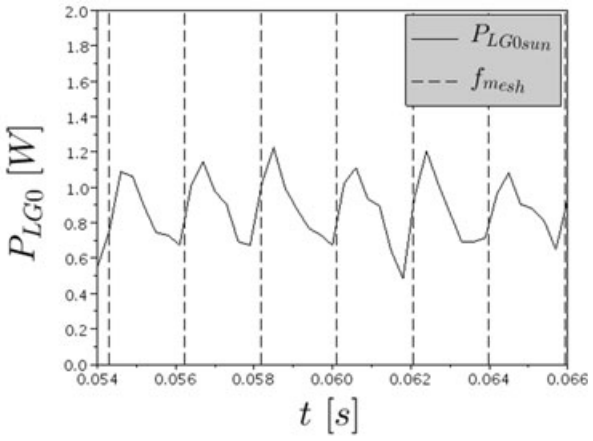

(F)

FIGURE 9 Two-dimensional simulation: ratio 10. Lubricant level: medium. A, Total hydraulic losses. B, Lubricant distribution. C, Planets power losses due to rotation. D, Planets power losses due to translation. E, Sun gear losses. F, Sun gear losses (detail) [Colour figure can be viewed at wileyonlinelibrary.com]

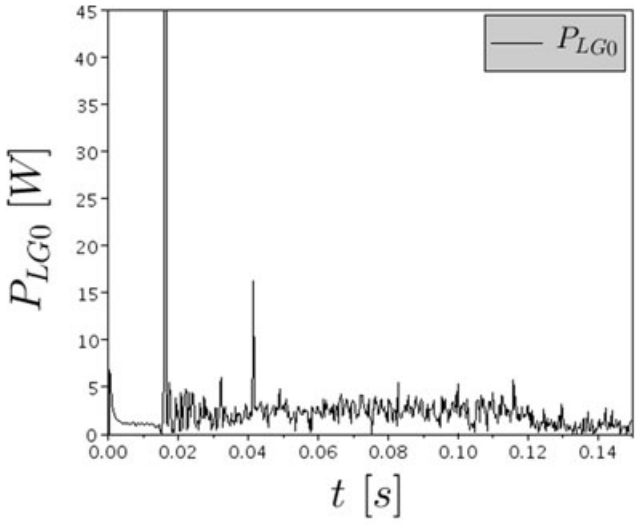

(A)

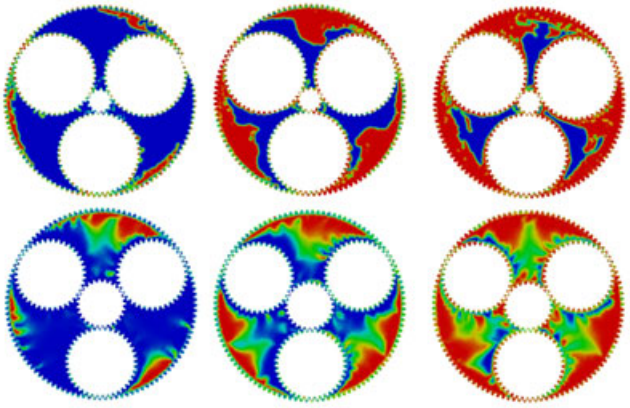

(B)

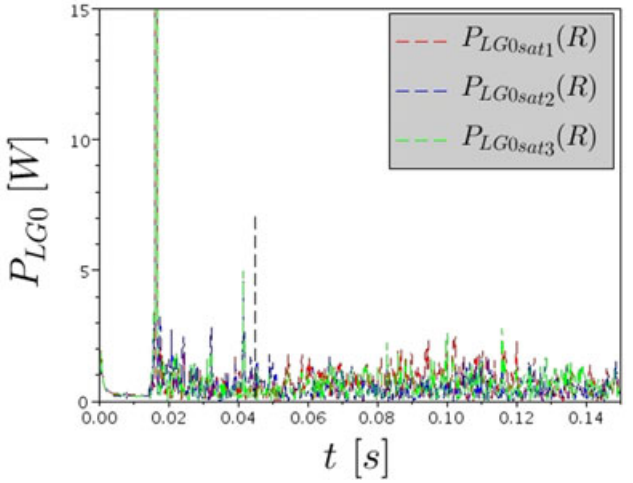

(C)

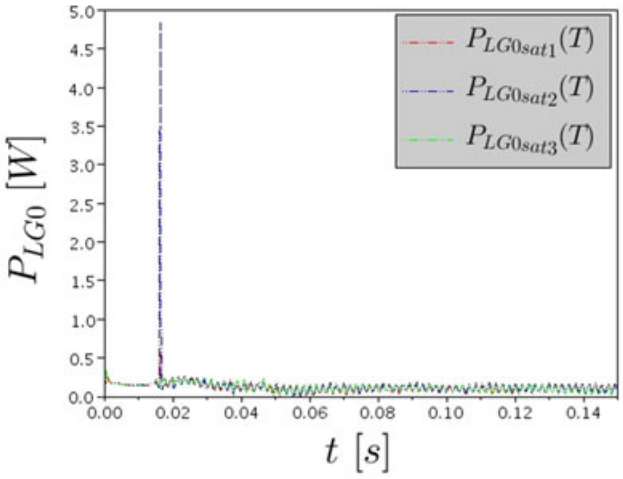

(D)

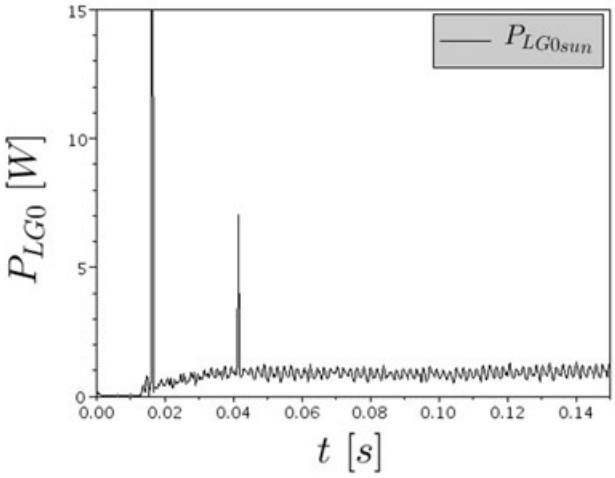

(E)

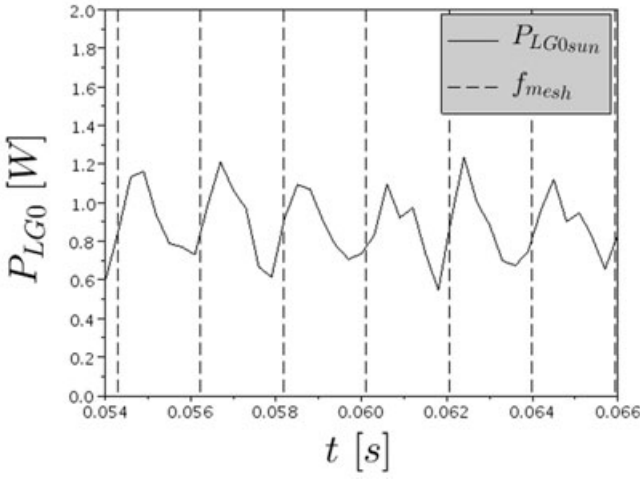

(F)

FIGURE 10 Two-dimensional simulation: ratio 10. Lubricant level: high. A, Total hydraulic losses. B, Lubricant distribution. C, Planets power losses due to rotation. D, Planets power losses due to translation. E, Sun gear losses. F, Sun gear losses (detail) [Colour figure can be viewed at wileyonlinelibrary.com]

This approach allows a mesh smoothing similar to the spring-based smoothing technique implemented in many commercial software. This method enables to keep the same mesh for a prescribed number of time steps. However, unavoidably the quality of the grid decreases and after some iteration, it should be substituted.

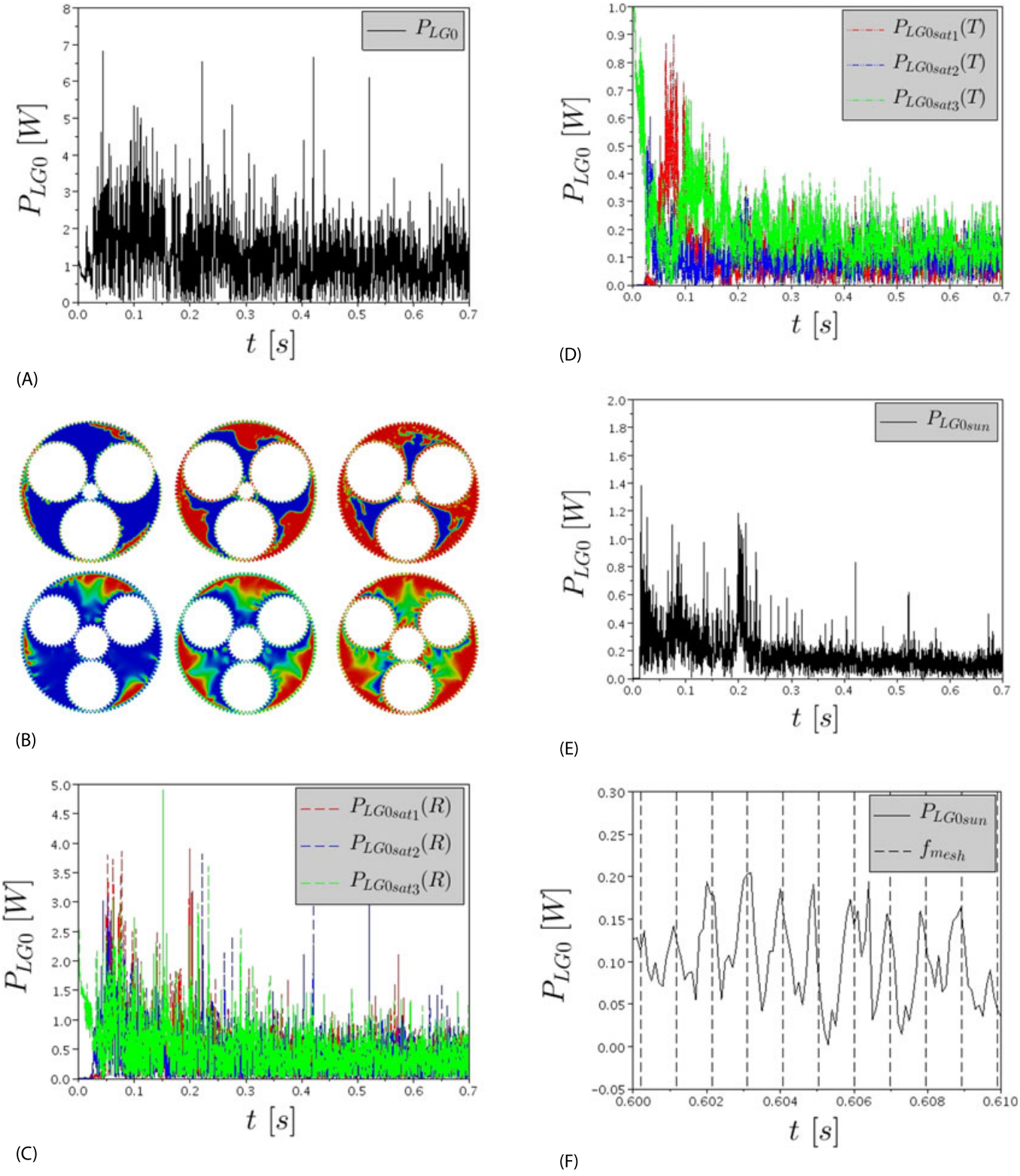

FIGURE 11 Two-dimensional simulation: ratio 5. Lubricant level: low. A, Total hydraulic losses. B, lubricant distribution. C, Planets power losses due to rotation. D, Planets power losses due to translation. E, Sun gear losses. F, Sun gear losses (detail) [Colour figure can be viewed at wileyonlinelibrary.com]

A new grid is generated only for the partitions which topology is changed (#2 to 6). The meshes are assembled and the filed variables mapped from the old and distorted grid to the new one. At this point, the simulation can restart. Figure 6A shows the flowchart of the simulation procedure.

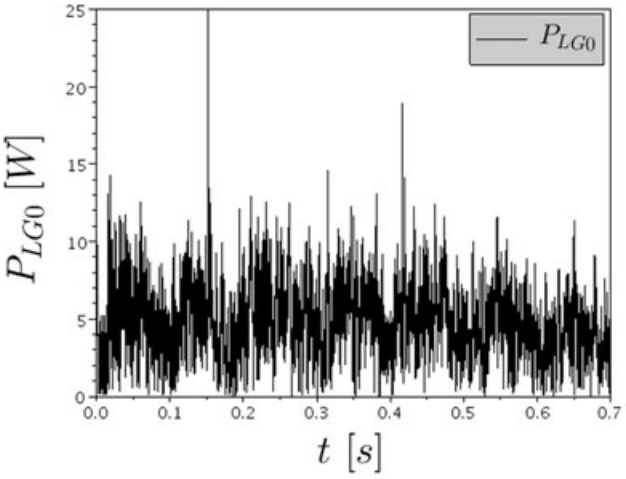

(A)

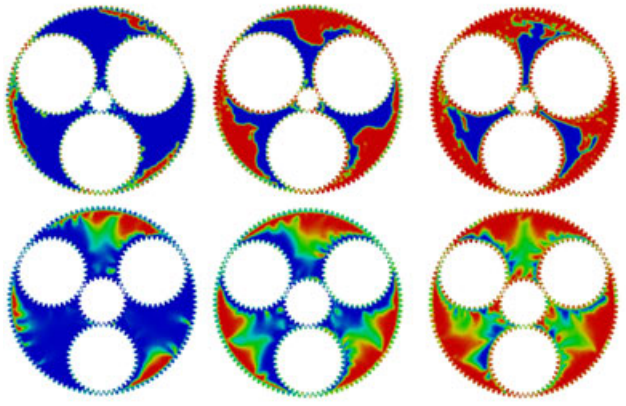

(B)

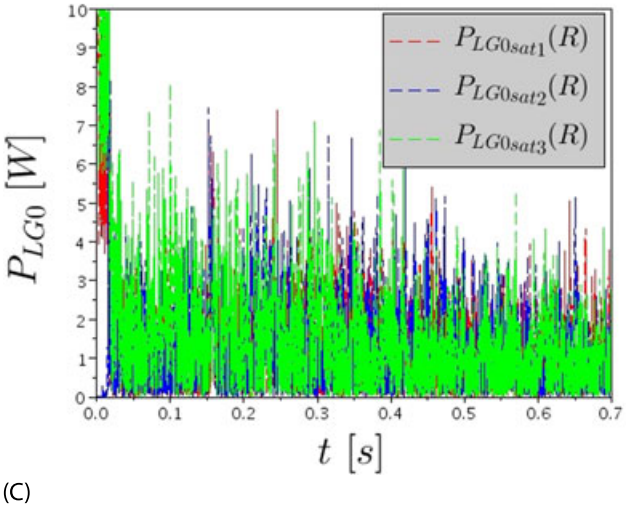

(C)

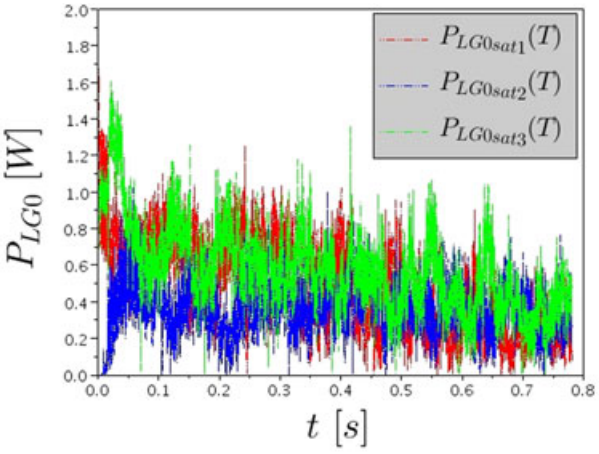

(D)

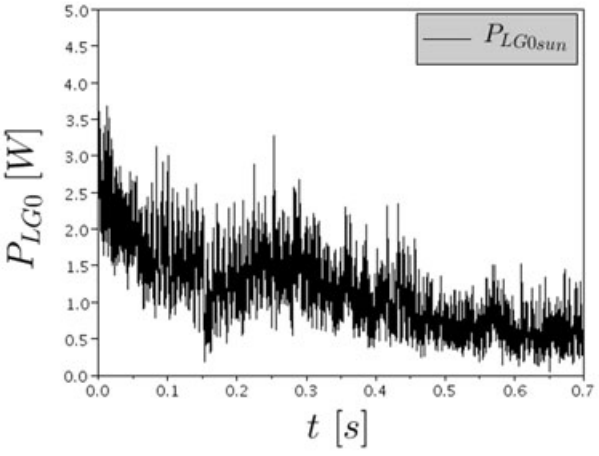

(E)

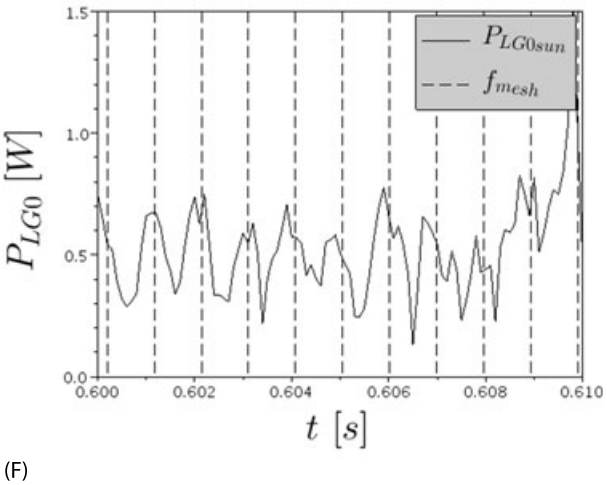

(F)

FIGURE 12 Two-dimensional simulation: ratio 5. Lubricant level: low medium. A, Total hydraulic losses. B, lubricant distribution. C, Planets power losses due to rotation. D, Planets power losses due to translation. E, Sun gear losses. F, Sun gear losses (detail) [Colour figure can be viewed at wileyonlinelibrary.com]

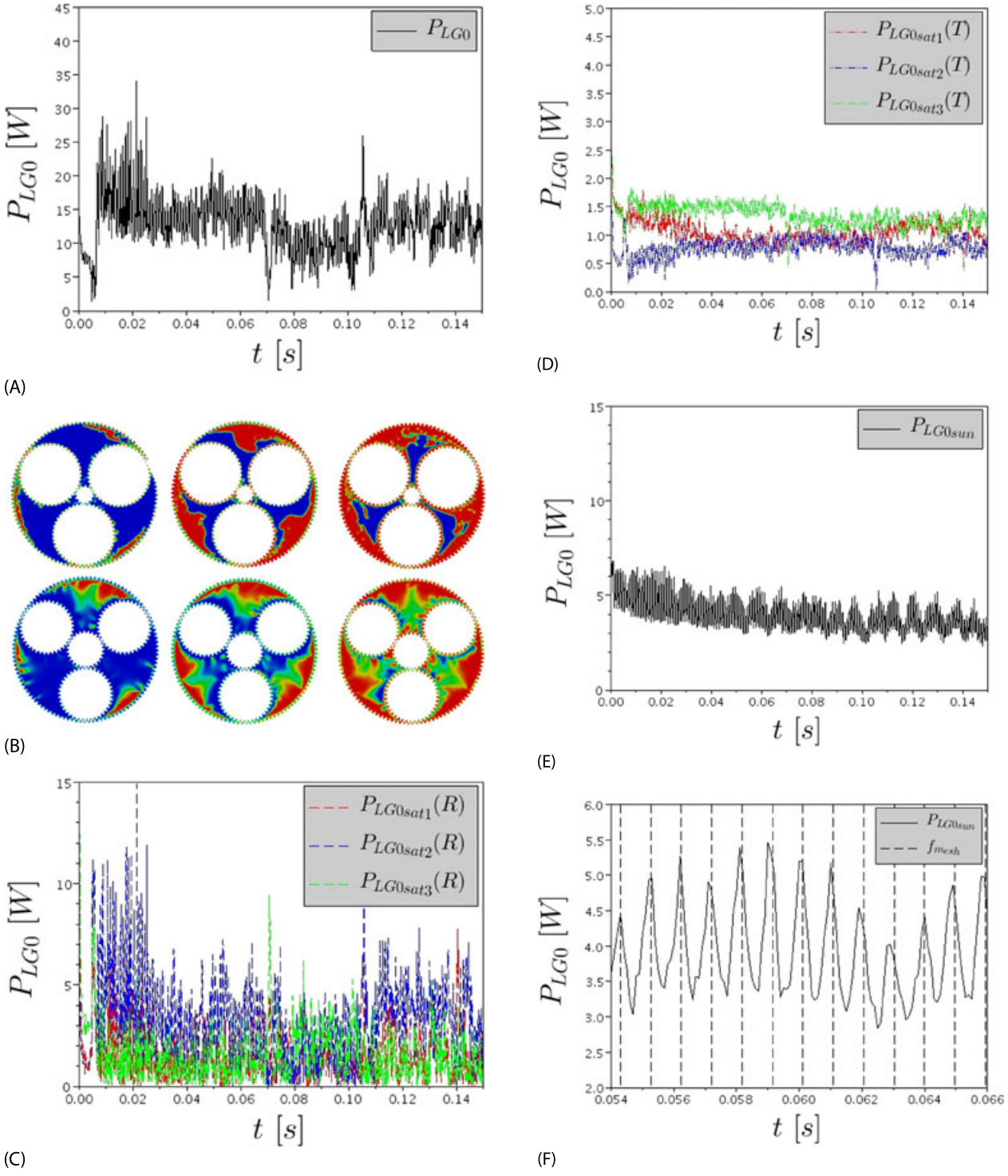

FIGURE 13 Two-dimensional simulation: ratio 5. Lubricant level: high. A, Total hydraulic losses. B, Lubricant distribution. C, Planets power losses due to rotation. D, Planets power losses due to translation. E, Sun gear losses. F, Sun gear losses (detail) [Colour figure can be viewed at wileyonlinelibrary.com]

2 | RESULTS AND DISCUSSION

2.1 | Two-dimensional simulations

Table 2 shows the power losses calculated with the 2D approximation. Besides increasing with the lubricant level, the results underline that while the planet carrier speed is limited (reduction ratio $i = 10$), the churning power losses are confined while when the rotational speed of the planet carrier increases ($\times 2$ with ratio $i = 5$), and the churning losses becomes significant and can not be neglected in a global efficiency calculation.

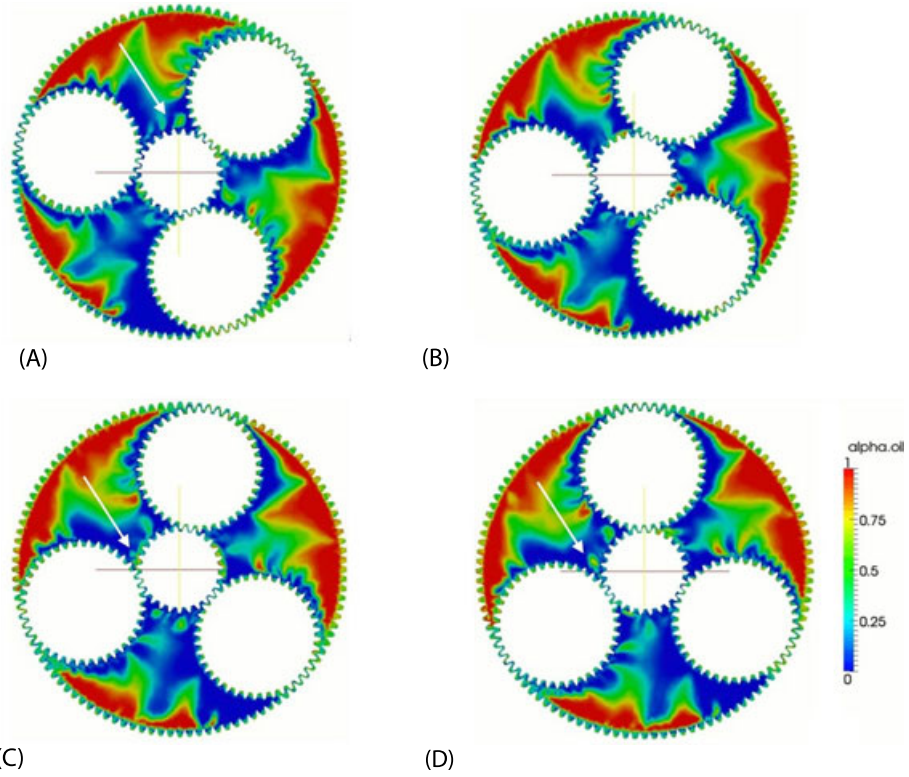

FIGURE 14 Detail of the squeezing effects: A, oil foam; B, the oil foam condensate in contact with the tooth; C, the oil droplet enters the contact; D, some foam is squeezed out from a backwards squeezing flow [Colour figure can be viewed at wileyonlinelibrary.com]

Dedicated tests under load ($n_1 = 3000rpm\,; C_2 = 16Nm$, *lub . level* 75%) on the gearbox with ratio 5 have shown that the total power dissipation is less than 125 W[30] also the highest lubricant level (Figure 7A). The measurements were performed on an energy-closed-loop test rig accurately described in Concli.[31] This evidence underlines the importance to be able to accurately predict the load independent power losses of gears to have a reliable estimation of the overall efficiency. The gear churning is responsible of the 22% of the total losses.

In a previous research,[17,18] the authors have experimentally tested a modified version of such reducer to measure the churning losses only (Figure 7B). From the comparison of the results of the 2D simulations and those measurements, it appears that while for high filling levels where the viscous contribution is negligible with respect to the inertial ones, the 2D approximations provides good results ($\text{err.l}_{\text{high}} = 3\%$), by reducing the lubricant level the viscous contribution cannot be anymore neglected. The results of the simulations show a significant underestimation of the experimental data ($\text{err.l}_{\text{med.}} = -27\%$ and $\text{err.l}_{\text{low}} = -66\%$).

Table 3 shows clearly the effect of the lubricant level on the churning losses shear. By incrementing the lubricant level, the contribution associated with the translation of the planets (T) becomes more significant with respect to the total dissipation of the planets. Furthermore, it can be seen that in the configuration with a smaller reduction ratio (higher speed of the planet carrier) this contribution is more significant. But while this additional churning can not be avoided, its effect can be significantly reduced just by reducing the lubricant level. A reduction of the oil filling from 75% to 50% (−33%: 37 ml less) produces a reduction of the churning losses from 15 to 5 W (−67%). The presented calculation tool can help in predicting

TABLE 4 Squeezing/pocketing loss shear for the sun gear

	$P_{LG0,sun,sq}/P_{LG0,sun}$ [−]	
Lubricant Level	$i = 10$	$i = 5$
Low	66%	90%
Medium	38%	40%
High	33%	20%

TABLE 5 Calculated power losses: 2D vs 3D simulations

$i = 10$ Lubricant Lev.: Med.	P_{LG0} [W]		ΔP_{LG0} [%] (2D vs 3D)
	2D	3D	
Sun	0.3	0.3	0%
Sat. rotation (R)	3 × 0.3	3 × 0.4	−25%
Sat. translation (T)	3 × 0.2	3 × 0.3	−33%
Planet carrier (PT)	-	1.1	-
TOT	2	3.5	−42%

Planet carrier is not modeled in the 2D approach: - stands for "no results available"

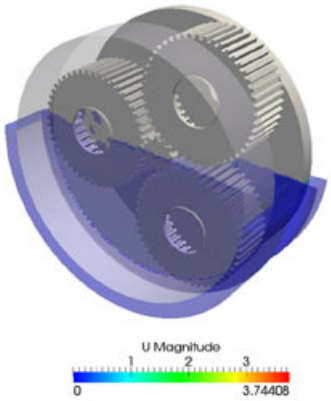

(A) Lubricant distribution (v [m/s])

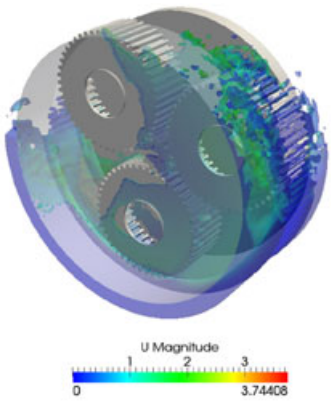

(B) Lubricant distribution (v [m/s])

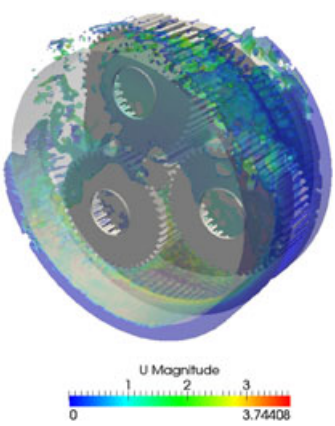

(C) Lubricant distribution (v [m/s])

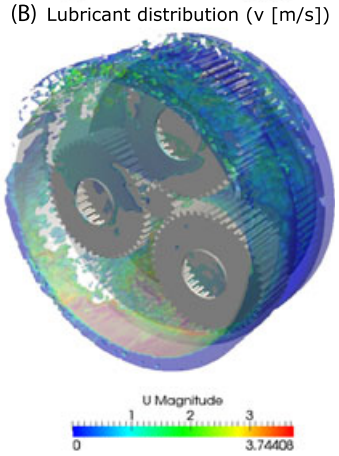

(D) Lubricant distribution (v [m/s])

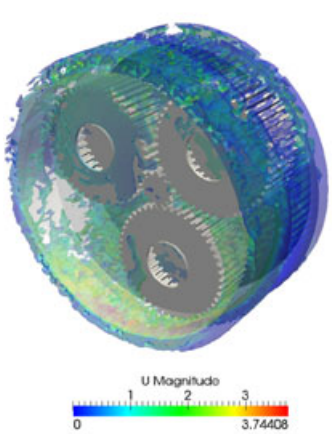

(E) Lubricant distribution (v [m/s])

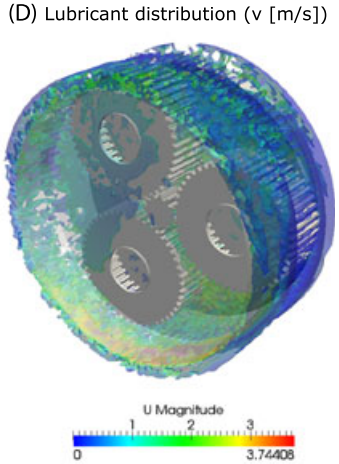

(F) Lubricant distribution (v [m/s])

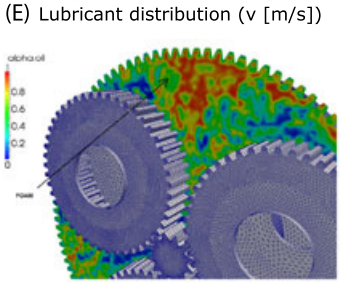

(G) volume fraction on the mid-plane and on the gear flanks [-]

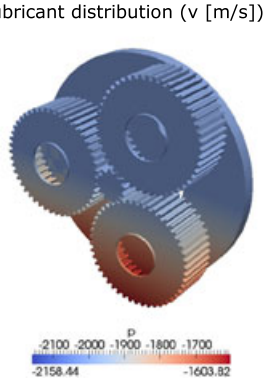

(H) pressure distribution on the boundaries [Pa]

FIGURE 15 A to F, Lubricant distribution (v [m/s]). H to M, Pressure distribution on the boundaries (Pa). G and N, Volume fraction on the midplane and on the gear flanks (–) [Colour figure can be viewed at wileyonlinelibrary.com]

the power losses as well as the efficiency and the temperatures under different conditions. This allows an optimization of the system targeted to find the best compromise between the reduction of the power losses achievable by reducing the amount of lubricant and the dissipation and cooling capability achievable, in turn, by adding more lubricant. Figures 8F to 13F show clearly how the resistant torque of the sun gear fluctuates around a mean value with a periodicity, which

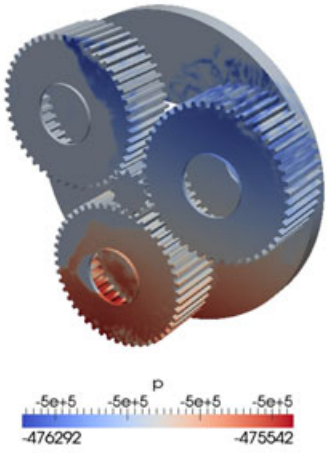

(I) pressure distribution on the boundaries [Pa]

(J) pressure distribution on the boundaries [Pa]

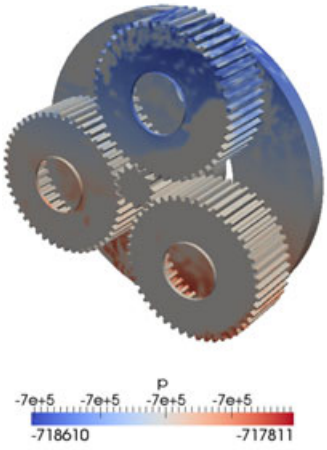

(K) pressure distribution on the boundaries [Pa]

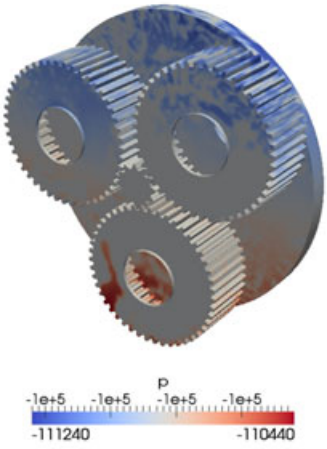

(L) pressure distribution on the boundaries [Pa]

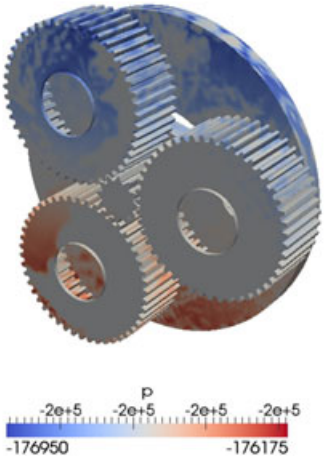

(M) pressure distribution on the boundaries [Pa]

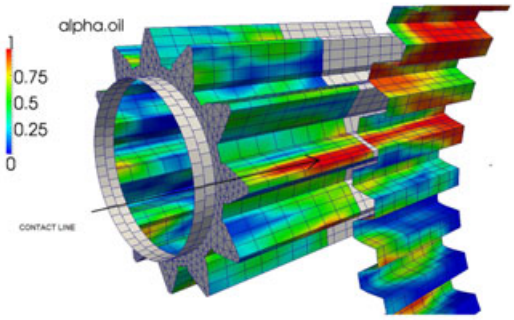

(N) volume fraction on the mid-plane and on the gear flanks [-]

FIGURE 15 (Continued)

frequency is the meshing frequency. While the mean value represent the churning power losses, the periodic fluctuations are due to the squeezing/pocketing effects.

This effect can also be observed in Figure 14.

Table 4 shows the shear of the squeezing losses (sq) among the total hydraulic losses of the sun gear. For both gearbox configurations, the squeezing losses becomes less significant by increasing the lubricant level due to the increase of the churning losses. This effect is more significant in the configuration with the smallest reduction ratio ($i = 5$), where the meshing frequency is double.

Furthermore, the total losses P_{LG0} show (Figure 8A to Figure 13A) another periodicity related to the rotational speed of the planet carrier ($T_{PT_{i=10}} = 1.93E{-}3\ s; T_{PT_{i=5}} = 9.6E{-}4\ s$). A secondary effect is related to the pass of the single planet ($T_{sat_{i=10}} = 6.9E{-}2\ s;\ T_{PT_{i=5}} = 3.4E{-}2\ s$) (Figure 14F).

2.2 | Three-dimensional simulations

Figure 15A to 15F shows the evolution of the lubricant distribution. Besides the acceleration of the fluids due to the rototranslation of the planets, Taylor-Couette flows[32] arise between the rotating sides of the planet carrier and counter plate and the fixed and planar internal surfaces of the housing as demonstrated by Durand de Gevigney et al.[33] These effects can be captured only with 3-dimensional simulations (Table 5). Figure 15G shows the lubricant distribution in the midplane after the regime condition is reached. The pure lubricant lies in proximity of the teeth of the ring gear due to the centrifugal effects caused by the rotation of the planets that induces a main circulation also in the lubricant. The air is mainly confined near the axis of the gearbox. In between a lubricant foam (air-lubricant mixture) generates. This foam is also present in the gaps between the teeth as shown experimentally by Chernoray.[34] Figure 15N shows clearly that when the gears mate, this foam condensates ensuring the separation of the gear flanks through the formation of a lubricant layer. This is fundamental to reduce the friction coefficient as well as to prevent damaging like wear and scuffing. Figure 15H to 15M shows the pressure distribution on the gears and the counter plate. Figure 15H represents the initial condition (the same as Figure 15A). The pressure is constant in the upper part of the gearbox that is filled with air. In the lower part in which the lubricant is present, the pressure increases downwards due to the self-weight of the oil. When the gears

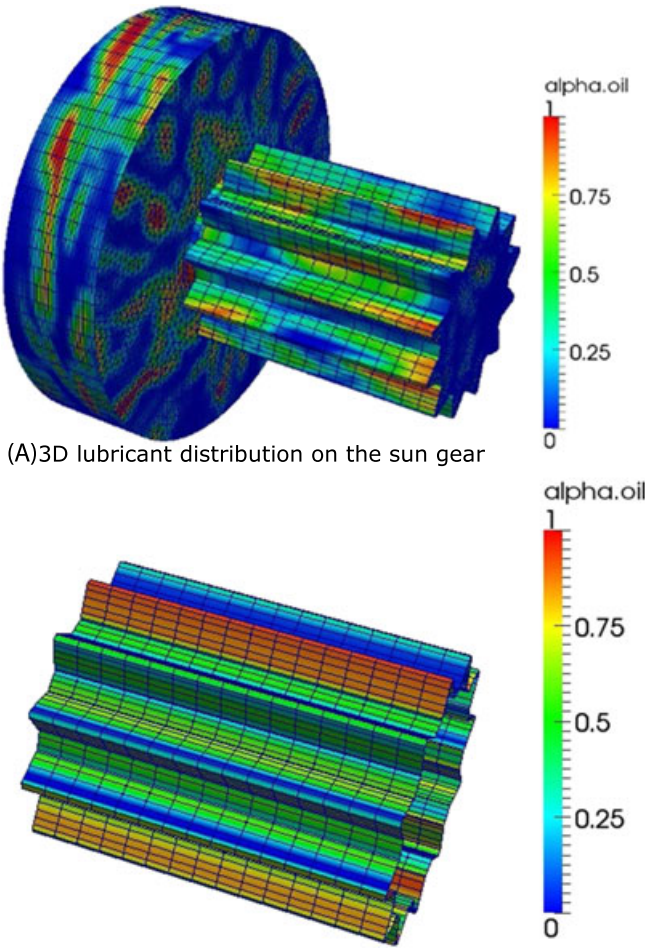

FIGURE 16 3D lubricant distribution on the sun gear and 2D approximation [Colour figure can be viewed at wileyonlinelibrary.com]

begin to rotate, the inertial effects of the lubricant causes pressure peaks on the boundaries. These effects can be easily seen comparing the lateral face of the upper planet of Figure 15F and Figure 15M. Significant pressure peaks are present only where the lubricant is present underlining that the air plays a lower order of magnitude role in the phenomenon of the power dissipation in dip-lubricated conditions as already demonstrated in Concli et al[20] (Figure 16a, 16b).

Figure 17 reports the results of the simulation of the gearbox configuration $i = 10$ and intermediate filling level. This should be compared to Figure 9 in terms of power losses.

The differences in the load-independent power losses of the planets between the 2- and 3-dimensional models are due to the additional lateral effects that are considered in the 3D model only. Furthermore the 3D model is capable to take into account also the power dissipation due to shear (viscous contribution) given by the planet carrier and mainly influenced by the induced Taylor-Couette flows.

Figure 17F shows a detail of the power losses generated by the translation of the planets at the beginning of the simulation. Satellites #1 and #2 lies in the oil bath, while satellite #3 lies in air. For this reason, only the contribution of the first 2 gears is significant. After 1/3 of rotation of the planet carrier, the configuration is similar but the satellite that lies in air and does not produce significant losses is #2. After another third of revolution is satellite #1 that lies in air. This

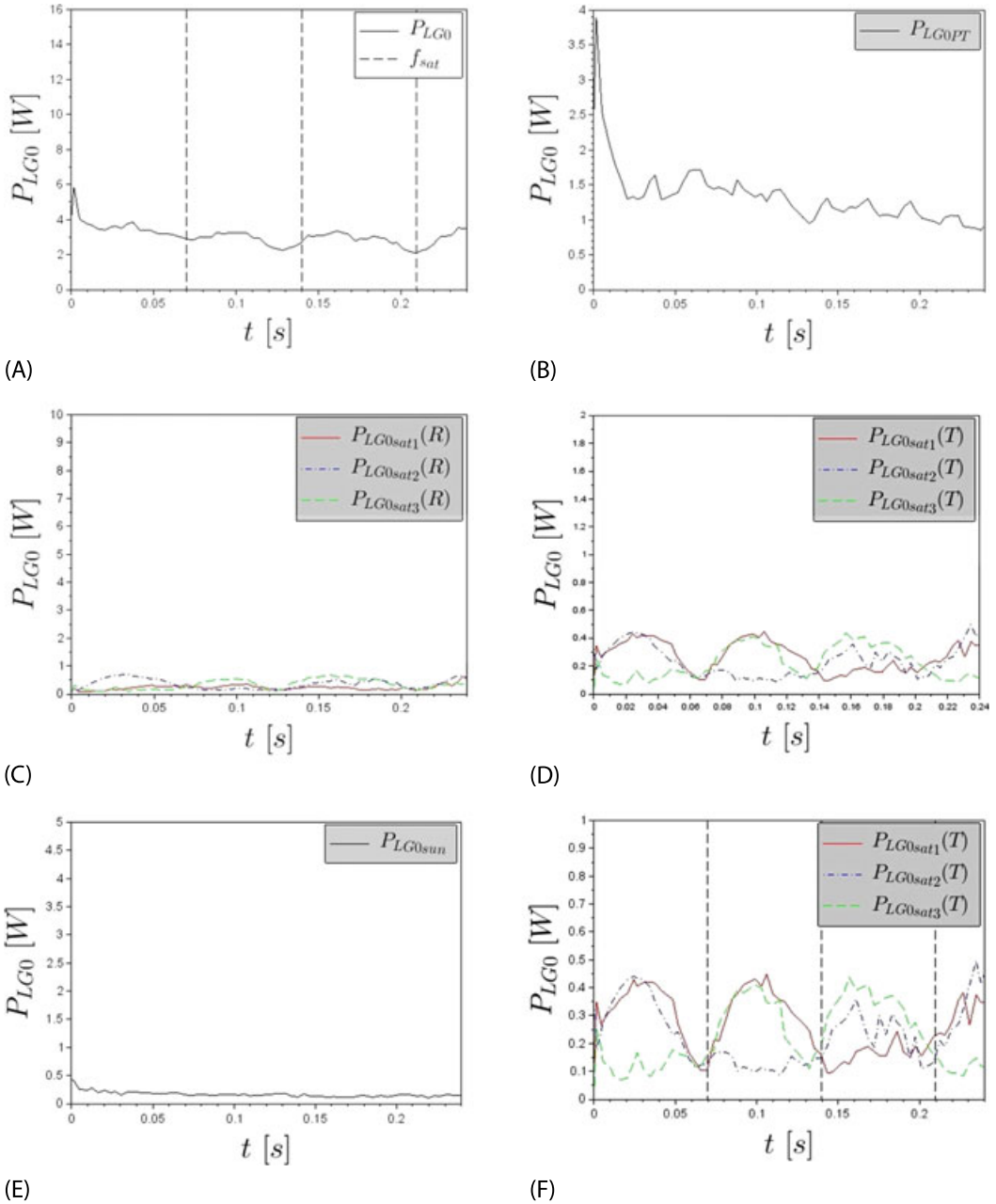

FIGURE 17 Three-dimensional simulation: ratio 10. Lubricant level: low [Colour figure can be viewed at wileyonlinelibrary.com]

phenomenon of attenuation of the losses for 1/3 of the revolution of the planet carrier becomes less significant after some rotations because air and lubricant will mix.

This explains how analytical model such as those proposed by Csobàn[35–38] that considers that the oil sump lies on the bottom of the gearbox, can be not accurate if the planet carrier speed is significant.

Besides the power loss and efficiency predictions, the method is capable to predict the lubricant fluxes, allowing to ensure the correct lubrication of all the mechanical components also with small amounts of oil.

2.3 | Performance enhancements

For the 2-dimensional simulations planar meshes of about 30k cells were used. The mesh size was chosen after a sensitivity analysis as the best compromise between the results accuracy and the computational effort. On a 211 GFLOPS workstation, each simulation took approximately 1 hour.

The shear of the computational effort between the different steps of the simulation can be evaluated as approximately 10% for the geometry generation, 15% for the mesh generation, 10% for the mapping of the fields from the old to the new meshes, and 65% for the solution of the internal fluid dynamics.

The final 3-dimensional mesh consists in approximately 1M cells. The simulation was performed the same 211 GFLOPS workstation used for the 2D simulations. The 3D simulation took approximatively 30 hours to reach the regime condition. The shear of the computational effort between the different steps of the simulation can be evaluated as approximately 5% for the geometry generation, 10% for the mesh generation, 10% for the mapping of the fields from the old to the new meshes, and 75% for the solution of the internal fluid dynamics.

3 | CONCLUSIONS

For the first time, CFD simulations were applied to planetary gears to study the internal lubrication and the related power dissipations without geometrical simplifications. This goal was achieved with an especially developed mesh-handling technique that regenerates the whole computational grid after few time steps to counteract the deformation induced by the boundary motion coupled with an innovative partitioning strategy. In the past, the authors tried without success to simulate the same configuration with commercial software but due to the huge computational effort it was not possible to complete the calculations. The new approach ensures a better control of the mesh quality with a big impact on the time step and, consequently, on the simulation time. The methodology applied to an FZG test rig ensures a simulation time reduction of about 93.5% with respect to commercial software.

The results of the 2D simulations are able to capture different phenomena among which churning and squeezing. On the other side, 2D simulations intrinsically neglect some contribution such those given by the lateral sides of the gears and by the planet carrier underrating the experimental data. This underestimation becomes less significant for high filling levels, while it cannot be neglected for low amounts of lubricant.

For this reason, an innovative automated partitioning strategy was implemented and coupled with the above described methodology. This lies on the axial subdivision of the domain so to be able to discretize each partition with a 2-dimensional extruded mesh. The different meshes are created separately. At the interfaces, the nonconformal grids are coupled with arbitrary numerical interfaces that ensure the continuity of the internal fields.

The results of the 3-dimensional simulation shows that the underestimation of the power losses is mainly due to Taylor-Couette flows that arise between the rotating sides of the planet carrier and the stationary internal surfaces of the housing. This result confirms the suggestion of other authors underlining how such new method can be used not only for an optimization of the gearbox design but also for a better comprehension of physical phenomena that can be hardy observed experimentally.

The methodology is fully parallelized and the reduced computational effort allows its application also in industrial application where the costs and the development times are priority.

REFERENCES

1. Daily J, Nece R. Chamber dimension effects of induced flow and frictional resistance of enclosed rotating disks. *ASME J Basic Eng*. 1960;82:217-232.
2. Mann R, Marston C. Friction drag on bladed disks in housings as a function of Reynolds number, axial and radial clearance, and blade aspect ratio and solidity. *ASME J Basic Eng*. 1961;83:719-723.
3. Soo SL, Princeton NJ. Laminar flow over an enclosed rotating disk. *Trans ASME*. 1958;80:287-296.
4. Terekhov AS. Hydraulic losses in gearboxes with oil immersion. *Vestnik Mashinostroeniya*. 1975;55:13-17.
5. Lauster E, Boos M. Zum Wärmehaushalt mechanischer Schaltgetriebe fьr Nutzfahrzeuge. *VDI-Ber.* 1983;488:45-55.
6. Boness RJ. Churning losses of discs and gears running partially submerged in oil. *Proc ASME Int Power Trans Gearing Conf, Chicago*. 1989;1:355-359.
7. Changenet C, Velex P. A model for the prediction of churning losses in geared transmissions—preliminary results. *ASME J Mech Des*. 2007;129(1):128-133.

8. Walter P, Langenbeck K. *Anwendungegrenzen für die Tauchschmierung von Zahnradgetrieben, Plansch- und Quetschverluste bei Tauchschmierung*. Frankfurt/M: Antriebstechnik; 1982.
9. Mauz W. *Hydraulische Verluste von Strinradgetrieben bei Umfansgsgeschwindigkeiten bis 60 m/s*. Stuttgart: IMK; 1987.
10. Gorla C, Concli F, Stahl K, et al. CFD simulation of splash losses of a gearbox. *Advances Tribol*. 2012; Article ID 616923, 10 pages.
11. Marchesse Y, Changenet C, Ville F, Velex P. Investigation on CFD simulations for predicting windage power losses on spur gears. *J Mech Des*. 2011;133: Article number 024501.
12. Hill MJ, Kunz RF, Medvitz RB, et al. CFD analysis of gear windage losses: validation and parametric aerodynamic studies. *J Fluid Eng*. 2011;133:
13. Gorla C, Concli F, Stahl K, et al. Hydraulic losses of gearbox: CFD analysis and experiments. *Tribol Int*. 2013;66:337-344.
14. Concli, F., Gorla, C., Analysis of the oil squeezing power losses of a spur gear pair by mean of CFD simulations, ASME 2012 11th Biennial Conference on Engineering Systems Design and Analysis, ESDA 2012; 2012 2, 177-184
15. Concli F, Gorla C. Oil squeezing power losses in gears: a CFD analysis. *WIT Trans Eng Sci.* 2012;74:37-48.
16. Gorla, C., Concli, F., Stahl, K., Höhn, B. R., Michaelis, K., Schultheiß, H., & Stemplinger, J.- P., Load independent power losses of ordinary gears: numerical and experimental analysis, 5th World Tribology Congress, WTC 2013; 2013 2, 1243-1246
17. Concli F, Gorla C, Conrado E. Analysis of power losses in an industrial planetary speed reducer: measurements and computational fluid dynamics calculations. *Proc Inst Mech Eng , Part J: J Eng Tribol*. 2014;228(1):11-21.
18. Concli F, Gorla C. Computational and experimental analysis of the churning power losses in an industrial planetary speed reducer. *WIT Trans Eng Sci*. 2012;74:287-298.
19. Concli F, Gorla C. Influence of lubricant temperature, lubricant level and rotational speed on the churning power loss in an industrial planetary speed reducer: computational and experimental study. *Int J Comput Methods Exp Meas*. 2013;1(4):353-366.
20. Concli F, Della Torre A, Gorla C, Montenegro G. Churning power losses of ordinary gears: a new approach based on the internal fluid dynamics simulations. *Lubr Sci*. 2015;27:313-326.
21. Concli F, Della Torre A, Gorla C, Montenegro G. A new integrated approach for the prediction of the power losses of gears: development of a mesh-handling algorithm to reduce the CFD simulation time. *Advances Tribol*. 2016; Article number 2957151.
22. Concli F, Gorla C. Numerical modeling of the power losses in geared transmissions: windage, churning and cavitation simulations with a new integrated approach that drastically reduces the computational effort. *Tribol Int*. 2016;103:58-68.
23. Niemann G, Winter H. *Maschinenelemente—Band 2: Getriebe Allgemein, Zahnradgetriebe— Grundlagen, Stirnradgetriebe—2*. Springer, Berlin, Germany: Auflage; 2003.
24. Ubbink O., Numerical prediction of the two fluid systems with sharp interfaces, Ph.D. Thesis, University of London; 1997.
25. Rusche H., Computational fluid dynamics of dispersed two-phase flows at high phase fractions, Ph.D. Thesis, Department of Mechanical Engineering, Imperial College of Science, Technology & Medicine, London; 2002.
26. Ansys Fluent, www.ansys.com
27. Netgen. www.hpfem.jku.at/netgen/
28. Schöberl J. *An advancing front 2D/3D–mesh generator based on abstract rules*. Computing and Visualization in Science, Germany: Springer; 1997.
29. Farrell PE, Maddison JR. Conservative interpolation between volume meshes by local galerkin projection. *Comput Methods Appl Mech Eng*. 2011;200:89-100.
30. OpenFOAM. http://www.openfoam.com
31. Concli F. Thermal and efficiency characterization of a low-backlash planetary gearbox: An integrated numerical-analytical prediction model and its experimental validation. *Proc IMechE Part J: J Eng Tribol*. 2016;230(8):996-1005.
32. Taylor GI. Stability of a viscous liquid contained between two rotating cylinders. *Phil Trans R Soc*. 1923;A223(605–615):289-343. Bibcode:1923RSPTA.223..289T. doi: 10.1098/rsta.1923.0008
33. Durand de Gevigney J, Changenet C, Ville F, Velex P, Becquerelle S. Experimental investigation on the no-load dependent power losses in a planetary gear set. *Int Conf Gears – VDI Berichte*. 2013;2199(2):1101-1112.
34. Chernoray V, Jahanmiri M. Experimental study of multiphase flow in a model gearbox. *WIT Trans Eng Sci*. 2011;70:153-164.
35. Csobán A, Kozma M. Influence of the oil churning, the bearing and the tooth friction losses on the efficiency of planetary gears. *Strojniski Vestnik/J Mech Eng*. 2010;56(4):231-238.
36. Csobán, A., Kozma, M., Investigation of the energy losses generated by the oil churning, the bearing and the tooth friction in planetary gear drives, 17th International Colloquium Tribology 2010 - Solving Friction and Wear Problems; 2010.
37. Csobán, A., Kozma, M., A model for calculating the oil churning, the bearing and the tooth friction losses generated in planetary gears, World Tribology Congress 2009 - Proceedings; 2009.
38. Csobán, A., Kozma, M., Influence of the power flow and the inner gear ratios on the efficiency of heavy-duty differential planetary gears, Technische Akademie Esslingen International Tribology Colloquium Proceedings; 2008.